

RESEARCH ARTICLE

Aggregation of CAT tails blocks their degradation and causes proteotoxicity in *S. cerevisiae*

Cole S. Sitron¹✉, Joseph H. Park^{1,2}✉, Jenna M. Giafaglione¹✉, Onn Brandman¹*✉

1 Department of Biochemistry, Stanford University, Stanford, CA, United States of America, **2** Department of Chemical & Systems Biology, Stanford University, Stanford, CA, United States of America

✉ These authors contributed equally to this work.

✉ Current address: Molecular Biology Interdepartmental Program, University of California Los Angeles, Los Angeles, CA, United States of America

* onn@stanford.edu.



OPEN ACCESS

Citation: Sitron CS, Park JH, Giafaglione JM, Brandman O (2020) Aggregation of CAT tails blocks their degradation and causes proteotoxicity in *S. cerevisiae*. PLoS ONE 15(1): e0227841. <https://doi.org/10.1371/journal.pone.0227841>

Editor: Eric Jan, University of British Columbia, CANADA

Received: October 10, 2019

Accepted: December 30, 2019

Published: January 16, 2020

Copyright: © 2020 Sitron et al. This is an open access article distributed under the terms of the [Creative Commons Attribution License](https://creativecommons.org/licenses/by/4.0/), which permits unrestricted use, distribution, and reproduction in any medium, provided the original author and source are credited.

Data Availability Statement: All relevant data are within the manuscript and its Supporting Information files.

Funding: This work was supported by Stanford University (O.B.), the US National Institutes of Health (grant No. R01GM115968 to O.B.), and the National Institute of General Medical Sciences of the US National Institutes of Health (grant No. T32GM007276 to C.S.S.). The funders had no role in study design, data collection and analysis, decision to publish, or preparation of the manuscript.

Abstract

The Ribosome-associated Quality Control (RQC) pathway co-translationally marks incomplete polypeptides from stalled translation with two signals that trigger their proteasome-mediated degradation. The E3 ligase Ltn1 adds ubiquitin and Rqc2 directs the large ribosomal subunit to append carboxy-terminal alanine and threonine residues (CAT tails). When excessive amounts of incomplete polypeptides evade Ltn1, CAT-tailed proteins accumulate and can self-associate into aggregates. CAT tail aggregation has been hypothesized to either protect cells by sequestering potentially toxic incomplete polypeptides or harm cells by disrupting protein homeostasis. To distinguish between these possibilities, we modulated CAT tail aggregation in *Saccharomyces cerevisiae* with genetic and chemical tools to analyze CAT tails in aggregated and un-aggregated states. We found that enhancing CAT tail aggregation induces proteotoxic stress and antagonizes degradation of CAT-tailed proteins, while inhibiting aggregation reverses these effects. Our findings suggest that CAT tail aggregation harms RQC-compromised cells and that preventing aggregation can mitigate this toxicity.

Introduction

Failed rounds of translation produce incomplete, potentially toxic polypeptides that organisms across all clades of life have evolved responses to degrade [1–5]. In prokaryotes, the primary degradative response involves a tRNA-mRNA hybrid molecule (tmRNA) [1]. The tmRNA enters stalled ribosomes, re-initiates translation elongation with its tRNA moiety and switches the ribosome's template to its mRNA moiety [1]. This prompts the ribosome to synthesize a tmRNA-encoded tag on the incomplete polypeptide's C-terminus that marks it for proteolysis [1]. The eukaryotic response, called Ribosome-associated Quality Control (RQC), begins when a set of factors recognize ribosomes that have stalled on the same mRNA and collided into each other [6–8]. These factors then split the ribosomes into their large and small

Competing interests: The authors have declared that no competing interests exist.

subunits, leaving the incomplete polypeptide (RQC substrate) tethered to the large subunit [9–17]. The E3 ligase Ltn1 binds to the large subunit and ubiquitylates the incomplete polypeptide, marking it for proteasomal degradation [10,18–21].

Disruption of tmRNA or Ltn1 compromises the cell's ability to degrade incomplete polypeptides and reduces survival under stresses that increase translational stalling [20,22–27]. This deficit in fitness at the cellular level has clinically-relevant consequences. tmRNA deficiency prevents growth of some disease-causing prokaryotes (e.g. *Mycoplasma genitalium* and *Staphylococcus aureus*) and decreases the virulence of others (e.g. *Salmonella enterica* and *Streptococcus pneumoniae*) [28–31]. In metazoan eukaryotes, mutations to *LTN1* or perturbations that introduce large influxes of RQC substrates lead to neurodegeneration [32–34]. Each of these phenotypes highlights the central role that tmRNA and Ltn1 play in maintaining protein homeostasis and avoiding the toxicity associated with compromised co-translational quality control.

A conserved back-up degradation pathway mediated by Rqc2 and its prokaryotic homologs mitigates some of the toxicity associated with loss of tmRNA or Ltn1 function [24,35]. Rqc2 homologs bind the large ribosomal subunit and direct it to elongate the incomplete polypeptide's C-terminus with either alanine (“Ala tails” in prokaryotes) or both alanine and threonine residues (“CAT tails” in yeast) [24,36,37]. Metazoan CAT tails may include a more diverse repertoire of amino acids [34]. These extensions, made without a small subunit or mRNA, act as “degrons” to mark incomplete polypeptides for degradation by the bacterial protease ClpXP or the eukaryotic proteasome [24,35].

Loss of Ltn1 function results in a buildup of CAT-tailed (“CATylated”) proteins [36]. The CAT tails on these proteins can homo-typically associate and form aggregates of CATylated proteins, which have been observed in yeast and metazoans [26,34,38,39]. The presence of threonine in yeast CAT tails increases their aggregation propensity [38]. It is thereby an attractive hypothesis that CAT tail aggregation has an adaptive function during stress. For instance, aggregation may protect the proteome by sequestering potentially harmful undegraded RQC substrates when Ltn1 becomes overburdened. Alternatively, it has been hypothesized that CAT tail aggregates disrupt cellular fitness by depleting the pool of chaperones [26,38,39], and thereby contribute to the proteotoxicity associated with Ltn1 failure. No study has evaluated these hypotheses by controlling the aggregation state of CAT tails and testing whether CAT tail aggregation plays a beneficial or harmful role during stress.

We used chemical and genetic approaches in *Saccharomyces cerevisiae* to modulate CAT tail aggregation propensity in Ltn1-deficient cells and determine how aggregation affects: 1) the function of CAT tails as degrons and 2) proteotoxic stress. We found that under conditions favoring CAT tail aggregation (elevated Rqc2 levels), CAT tails lose their degron function and induce proteotoxic stress. Conversely, we observed that increasing CAT tail solubility (with guanidinium hydrochloride or by genetic perturbation of RNA Polymerase III function) restores CAT tail-mediated degradation and reduces proteotoxic stress. Our work demonstrates that CAT tail aggregation contributes to the toxicity of Ltn1 disruption rather than aiding in adaptation to stress.

Materials and methods

Yeast strains and culturing

The parental wild-type yeast strain used in this study was BY4741. All gene deletions, genomic integrations, and plasmid transformations were done in this background using standard methods. For a complete list of strains used, see [S1 Table](#).

Yeast cultures were grown at 30°C in YPD or synthetic defined (SD) media with appropriate nutrient dropouts. SD media used for growth of yeast cultures contained: 2% w/v dextrose (Thermo Fisher Scientific, Waltham, MA), 13.4 g/L Yeast Nitrogen Base without Amino Acids (BD Biosciences, San Jose, CA), 0.03 g/L L-isoleucine (Sigma-Aldrich, St. Louis, MO), 0.15 g/L L-valine (Sigma-Aldrich), 0.04 g/L adenine hemisulfate (Sigma-Aldrich), 0.02 g/L L-arginine (Sigma-Aldrich), 0.03 g/L L-lysine (Sigma-Aldrich), 0.05 g/L L-phenylalanine (Sigma-Aldrich), 0.2 g/L L-Threonine (Sigma-Aldrich), 0.03 g/L L-tyrosine (Sigma-Aldrich), 0.018 g/L L-histidine (Sigma-Aldrich), 0.09 g/L L-leucine (Sigma-Aldrich), 0.018 g/L L-methionine (Sigma-Aldrich), 0.036 g/L L-tryptophan (Sigma-Aldrich), and 0.018 g/L uracil (Sigma-Aldrich). Media additionally contained 5 mM or 10 mM guanidinium hydrochloride (Sigma-Aldrich) where indicated and bortezomib (LC Laboratories, Woburn, MA) treatment lasted 4 hours.

Plasmids

Plasmids were constructed using NEBuilder HiFi DNA Assembly Master Mix (New England Biolabs, Ipswich, MA). All plasmids used in this study are described in [S2 Table](#).

Two variants of RQCsub were used that had identical construction except for the region following the stall: one had a fluorescent protein (RFP) and the other had a series of affinity tags. The version without the post-stall RFP was used for microscopy and the version with the post-stall RFP was used in immunoblots.

Flow cytometry

Fluorescence was measured using a BD Accuri C6 flow cytometer (BD Biosciences). Three independent yeast cultures were grown to log phase overnight in appropriate SD dropout media. Data analysis was performed with MATLAB (MathWorks, Natick, MA).

For measurements of the Hsf1 activity reporter, raw fluorescence values were first normalized to side scatter, \log_2 -transformed, and then the value obtained from the wt strain was subtracted from each condition. These calculations are reported as \log_2 fold wt in the figures.

For measurements of RQCsub_{LONG}, a detailed description of the analysis workflow can be found in [35]. Briefly, yeast expressing the plasmid were gated according to above-background RFP fluorescence. Then, bleedthrough from the RFP channel was calculated using an RFP-only control strain and subtracted from signal in the GFP channel. The resultant bleedthrough-corrected GFP:RFP values were normalized to the corresponding untreated *hul5Δ* strain for each background. To quantify the change in GFP:RFP upon *HUL5* deletion, the normalized value from the *HUL5* condition was subtracted from that of the *hul5Δ* condition.

For the stalling reporter, the analysis workflow matched that of RQCsub_{LONG} with the order of the fluorophores being reversed, i.e. plasmid-expressing yeast selected based on GFP, bleedthrough from GFP subtracted from RFP. Where indicated, corrected RFP:GFP values were normalized to a non-stalling reporter that contained a non-stalling sequence encoding serine and threonine [17] in place of the stalling CGN codons.

Statistical analysis

A paired t-test (using the “ttest” function in MATLAB) was used to assess whether mean measurements differed between two different conditions, using the null hypothesis: $\mu_{\text{condition 1}} = \mu_{\text{condition 2}}$. To calculate the s.e.m. for Δ stability measurements, a propagation of error formula was used: $SEM_{hul5\Delta-HUL5} = \sqrt{SEM_{HUL5}^2 + SEM_{hul5\Delta}^2}$. To analyze the significance of Δ stability measurements, a t-test for particular contrast was performed using the “lm” and

“linearHypothesis” functions in R (R Foundation for Statistical Computing). The null hypothesis for this test was: $\mu_{hul5\Delta+ \text{ condition 1}} - \mu_{HUL5+ \text{ condition 1}} = \mu_{hul5\Delta+ \text{ condition 2}} - \mu_{HUL5+ \text{ condition 2}}$.

Immunoblots

For whole-cell immunoblots, 0.375/OD600 x mL of yeast culture (OD600 = 0.4–0.8) grown overnight were pelleted and resuspended then boiled for 5 min at 95°C in 15 μ L 4x NuPage LDS Sample Buffer (Thermo Fisher Scientific) with 5% β -mercaptoethanol.

For SDS-PAGE, samples were loaded into a NuPAGE Novex 4–12% Bis-Tris 1.5 mm protein gel (Thermo Fisher Scientific) and run in MOPS buffer. Gels were semi-dry transferred to 0.45 μ m nitrocellulose membranes (Thermo Fisher Scientific) using the Trans-Blot Turbo system (Bio-Rad, Hercules, CA). Gels were wet transferred to .45 μ m nitrocellulose membranes (Thermo Fisher Scientific) in the Trans-Blot Cell (Bio-Rad) in Towbin Buffer or semi-dry transferred using a Trans-Blot Turbo (Bio-Rad).

Membranes were blocked in TBST with 5% fat-free milk (Safeway, Pleasanton, CA) for 1 hour, incubated overnight at 4°C or at room temperature for 4 hrs in one of the following primary antibodies: 1:3000 mouse α -GFP (MA5-15256, Thermo Fisher Scientific), 1:3000 rabbit α -hexokinase (H2035-01, US Biological, Salem, MA), or 1:1000 rabbit α -RFP (AB233, Evrogen, Moscow, Russia). The following secondary antibodies were then used at 1:5000 dilution: IRDye 800CW donkey anti-mouse, IRDye 800CW goat anti-rabbit, IRDye 680RD goat anti-rabbit, or IRDye 680RD goat anti-mouse (LiCor Biosciences, Lincoln, NE). Blots were scanned on a Licor Odyssey (LiCor Biosciences).

Lysate preparation and immunoprecipitation (IP)

Yeast were grown in SD media and harvested at OD600 0.8 to 1.0. Cells were harvested using either 1) centrifugation followed by resuspension in IP buffer (100 mM KOAc, 10 mM MgCl₂, 25 mM HEPES-KOH pH 7.4) and freezing of cell droplets in liquid nitrogen; or 2) vacuum filtration and flash freezing in liquid nitrogen. Frozen yeast were cryogenically pulverized into powder using a Freezer/Mill (SPEX SamplePrep, Metuchen, NJ) and stored at -80°C.

Frozen yeast powder was thawed and solubilized at 4°C in IP buffer supplemented with Pierce Protease Inhibitor Tablets, EDTA-free (Thermo Fisher Scientific). Crude lysate was clarified by a single spin at 5000 x g. For lysate immunoblots, this lysate was denatured by addition of 4X NuPAGE LDS Sample Buffer with 5% β -mercaptoethanol and boiling, then analyzed as described above in “Immunoblots.” For immunoprecipitations, the lysate was incubated with GFP-Trap_A (ChromoTek, Planegg-Martinsried, Germany) resin for 1 hour at 4°C with rotation, then washed 10 times in IP buffer. For immunoblotting, washed GFP-Trap resin was boiled in 4X NuPAGE LDS Sample Buffer (Thermo Fisher Scientific) with 5% β -mercaptoethanol and analyzed as described above in “Immunoblots.”

TEV protease digestion

GFP IP was performed as described above, but instead of immediate elution, the resin was equilibrated in IP buffer with 1 mM DTT and incubated overnight at 4°C with 5 μ L ProTEV Plus (Promega, Sunnyvale, CA) in 100 μ L total reaction volume. The resin was then washed with fresh IP buffer with 1 mM DTT and boiled in 4X NuPAGE LDS Sample Buffer (Thermo Fisher Scientific) with 5% β -mercaptoethanol and analyzed as described above.

Fluorescence microscopy

Live cell fluorescence imaging was performed using two set-ups: 1) a Nikon Eclipse Ti-E inverted fluorescence microscope (Nikon, Melville, NY) using a 100X/1.4NA oil objective lens and μ Manager [40], and 2) a Nikon Eclipse 80i microscope using a 100X/1.4NA oil objective lens and Metamorph (Molecular Devices, San Jose, CA). Yeast were grown in SD media to log phase, centrifuged briefly, resuspended in 5 μ L fresh SD media and mounted on a clean coverslip and slide. Images were prepared and analyzed with ImageJ (NIH). For quantification, images were randomly acquired until $N > 300$ cells. Independent cultures were imaged on different days and error represents standard deviation of 3 independent cultures.

Yeast spot assay

Yeast were grown to log-phase in YPD, then diluted to $OD_{600} = 0.1$. 200 μ L of this diluted culture was diluted 1:10 into YPD four times in a sterile 96-well plate (Greiner Bio-one, Kremsmünster, Austria). 5 μ L of the serial dilutions were transferred from the 96-well plate onto YPD agar plates with or without 5 mM guanidinium hydrochloride (Sigma-Aldrich), 50 ng/mL cycloheximide (Sigma-Aldrich) (with and without additional 5 mM guanidinium hydrochloride), 1.5 mM paromomycin (Chem-Impex International, Wood Dale, IL), 50 μ g/ml hygromycin B (Goldbio, St. Louis, MO). Plates were then incubated at 30°C or 37°C. Plates grown at 30°C with or without 5 mM guanidinium hydrochloride as well as 37°C plates were imaged after two days. Plates containing 50 ng/mL cycloheximide (with or without 5 mM guanidinium hydrochloride), 1.5 mM paromomycin, 50 μ g/ml hygromycin B, grown at 30°C were imaged after three days. Plates with 5 mM guanidinium hydrochloride grown at 37°C were imaged after six days.

Hsf1 reporter screen

Approximately 6,000 MATa strains carrying unique KanR-selected loss-of-function alleles were crossed to two strains with integrated Hsf1 reporters in the Y8091 background (MAT α *his3 Δ 1 leu2 Δ 0 URA3::4xHSE-EmGFP cyh2 can1 Δ ::STE2pr-spHIS5 lyp1 Δ ::STE3pr-LEU2* and MAT α *his3 Δ 1 leu2 Δ 0 ura3 Δ 0 rps0a::URA3-4xHSE-EmGFP cyh2 can1 Δ ::STE2pr-spHIS5 lyp1 Δ ::STE3pr-LEU2 ltn1 Δ ::natMX*) [19] using the Synthetic Genetic Array methodology [41]. The result of these crosses were two groups of strains: loss-of-function Hsf1 reporter strains with and without deletions of *RPS0A* and *LTN1*. These two groups of strains were measured once via flow cytometry on a BD LSR II flow cytometer (BD Biosciences). The data was analyzed as described above and is reported in [S1 Dataset](#), with hypomorphs lacking at least 30 cells excluded.

Results

CAT tail aggregation is associated with compromised CAT tail degradation

We began our investigation into the effects of aggregation on CAT tail-mediated degradation by validating the model RQC substrate RQCsub. RQCsub consists of green fluorescent protein (GFP) attached via an inert linker including a tobacco etch virus (TEV) protease site to twelve stall-inducing arginine CGN codons (Fig 1A) [42]. Translation of RQCsub produces a stalled GFP-linker-arginine “arrest product” [19]. The RQCsub arrest product accumulated at low levels in wt strains by SDS-PAGE (Fig 1A). The arrest product increased in abundance after we compromised RQC function by deleting either of two RQC genes: the CAT tail-elongating factor *RQC2* or the E3 ubiquitin ligase *LTN1* (Fig 1A). This result indicates that Rqc2 and Ltn1 contribute to RQCsub degradation. While deletion of *RQC2* or *LTN1* stabilized RQCsub, the

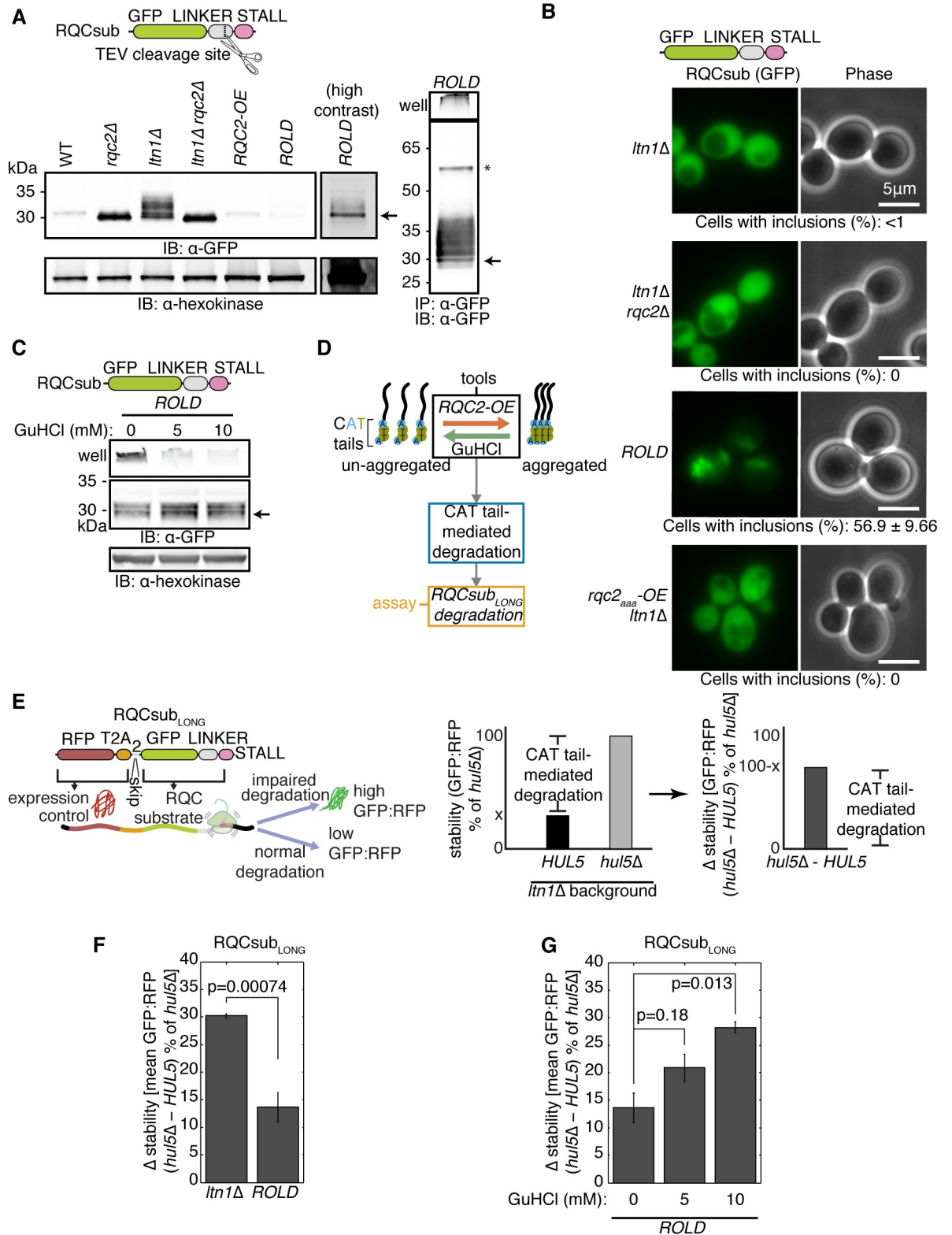


Fig 1. Aggregation compromises CAT tail degradation. (A) Left, whole cell immunoblots (IBs) of lysates containing the model RQC substrate RQCsub (schematic above). Right, IB of RQCsub immunoprecipitated (IPed) from *RQC2* overexpression and *LTN1* deletion (*ROLD*) lysate. Arrow indicates molecular weight of RQCsub without CAT tails. Asterisk denotes the full-length RQCsub protein product, produced when ribosomes translate through the stall sequence (region past the stall not pictured in schematic). GFP, green fluorescent

protein. OE, overexpression. (B) Fluorescence microscopy of cells expressing RQCsub with percentages of cells containing observable GFP inclusions reported below. (C) IB of RQCsub from *ROLD* lysates derived from cultures grown in guanidinium hydrochloride (GuHCl). Arrows as in A. (D) Schematic of experimental approach for measuring the effect of aggregation of CAT tail-mediated degradation. (E) Left, schematic of expression-controlled model RQC substrate RQCsub_{LONG}. Center, definitions of “stability,” “Δ stability,” and “CAT tail-mediated degradation.” (F) and (G) Δ stability measurements of RQCsub_{LONG} expressed in *ltn1Δ* and *ROLD* cells after *HUL5* deletion to assess CAT tail degron activity. P-values above bars are derived from t-tests for particular contrast, measuring how significantly different *HUL5* deletion-induced stabilization is between either *ltn1Δ* and *ROLD* backgrounds in F or between different GuHCl concentrations in G. Error bars represent the standard error of the mean (s.e.m.).

<https://doi.org/10.1371/journal.pone.0227841.g001>

resultant protein products displayed different mobilities: RQCsub from *rqc2Δ* cells migrated as a crisp band and that from *ltn1Δ* cells migrated as a higher molecular weight smear (Fig 1A). This smear collapsed into a single band after additional deletion of *RQC2* in the *ltn1Δ* strain (Fig 1A), consistent with the smear containing CATylated RQCsub. Taken together, these results confirm that RQCsub is degraded via RQC and CATylated by Rqc2.

To vary the aggregation propensity of CAT tails, we overexpressed *RQC2*, which has previously been shown to increase CAT tail aggregation [38]. Overexpression of *RQC2* with the *TDH3* promoter increased Rqc2 levels 28.4-fold relative to the native promoter, as assessed by levels of red fluorescent protein (RFP)-tagged Rqc2 (S1 Fig panel A). In the *RQC2* overexpression and *LTN1* deletion strain (hereafter named “*ROLD*”), a proportion of RQCsub remained in the well rather than migrating into an SDS-PAGE gel (Fig 1A) despite prior boiling in dodecylsulfate detergent. This detergent-resistant species was more prominent in *ROLD* than in *ltn1Δ* lysates or lysates from cells with *RQC2* overexpression alone (“*RQC2-OE*”) (S1 Fig panel B). TEV treatment, which cleaves RQCsub’s C-terminus to remove its CAT tail, enabled RQCsub purified from *ROLD* cells to migrate as a single band into the gel (S1 Fig panel C). The properties of this detergent-resistant species are consistent with *RQC2* overexpression reducing the solubility of CATylated RQCsub in the *ltn1Δ* background. Microscopy revealed that RQCsub had a diffuse localization in the majority of *ltn1Δ* cells (<1% of cells with inclusions) but became more punctate in *ROLD* cells (56.9% of cells with inclusions) (Fig 1B). To test whether these inclusions depended on CATylation, we disrupted CATylation by deleting *RQC2* or overexpressing a CATylation-incompetent *rqc2_{aaa}* allele [36] instead of *RQC2-WT*. Neither of these perturbations (*rqc2Δ ltn1Δ* nor *rqc2_{aaa}-OE ltn1Δ*) induced the punctate RQCsub localization we observed in *ROLD* cells (Fig 1B), confirming that formation of RQCsub inclusions requires CATylation. These results demonstrate that the *ROLD* genetic background can be used to enhance CAT tail aggregation.

We next sought a tool to inhibit CAT tail aggregation. Millimolar concentrations of the chaotrope guanidinium hydrochloride (GuHCl) in yeast growth medium limit CAT tail aggregation and block propagation of aggregated yeast prions by inhibiting the ATPase activity of the chaperone Hsp104 [39,43–49]. When we treated *ROLD* cells with GuHCl, we observed that RQCsub still localized to inclusions by microscopy (S1 Fig panel D). However, monitoring RQCsub mobility in SDS-PAGE assessed how GuHCl affected RQCsub more sensitively than microscopy, revealing that GuHCl treatment enabled a larger proportion of RQCsub extracted from *ROLD* cells to migrate into the resolving gel rather than remaining in the well (Fig 1C). The presence of GuHCl in growth medium thus reduces the detergent insolubility of CAT tails and can thereby serve as a tool to inhibit CAT tail aggregation.

Single-color model RQC substrates like RQCsub, while useful for visualizing CAT tails by SDS-PAGE and microscopy, have limited utility in degradation measurements due to noisy expression [35]. To assess how aggregation affects degradation of CATylated RQC substrates, we utilized the two-color model RQC substrate RQCsub_{LONG} [35] (Fig 1D and 1E). RQCsub_{LONG} includes an internal expression control, RFP followed by viral T2A peptides, at the N-

terminus of GFP-linker-arginine (Fig 1E). Ribosomes translating RQCsub_{LONG} produce RFP then skip formation of a peptide bond within the T2A sequence [50,51], severing RFP from the GFP-linker-arginine RQC substrate (Fig 1E). As a result, each round of translation produces RFP and GFP stoichiometrically, but only GFP becomes an RQC substrate (Fig 1E). When we analyzed GFP and RFP separately, we observed that each signal was lower in *ROLD* than in *ltn1Δ* cells (S2 Fig panel A). This loss of fluorescent signal was especially evident for the expression control RFP (S2 Fig panel A), indicative of reduced RQCsub_{LONG} translation in the *ROLD* background. This reduction in translation may explain why we observed lower RQCsub levels in the *ROLD* background compared to *ltn1Δ* by SDS-PAGE (Fig 1A) and highlights the need for a precise way to measure degradation that is not confounded by changes in translation.

We then controlled for these differences in translation to quantify how increased CAT tail aggregation (in the *ROLD* strain) affects degradation of CATylated RQCsub_{LONG}. The ratio of GFP:RFP at the single-cell level serves as an internal, expression-controlled readout of RQCsub_{LONG} stability (Fig 1E). CAT tail-mediated degradation of RQCsub_{LONG} in the absence of Ltn1 requires the proteasome-associated E3 ubiquitin ligase Hul5 and the proteasome [35]. Therefore, comparing stability before and after *HUL5* deletion quantifies CAT tail-mediated degradation (Fig 1E). RQCsub_{LONG} stability did not change after treatment of *ltn1Δ hul5Δ* or *ROLD hul5Δ* cells with the proteasome inhibitor bortezomib (S2 Fig panel B), supporting the requirement for Hul5 in CAT tail-mediated degradation of RQCsub_{LONG} by the proteasome. *HUL5* deletion stabilized RQCsub_{LONG} by 30.2% in *ltn1Δ* and 13.6% in *ROLD* backgrounds (Fig 1F), consistent with *RQC2* overexpression reducing CAT tail-mediated RQCsub_{LONG} degradation. These results demonstrate that the *ROLD* genetic background, which potentiates CAT tail aggregation, impairs CAT tail-mediated degradation.

To ensure that it is aggregation (and not another effect of *ROLD*) that reduces CAT tail-mediated degradation, we inhibited aggregation with GuHCl and measured RQCsub_{LONG} stability. We observed that GuHCl treatment had two effects on RQCsub_{LONG} degradation in *ROLD* strains. First, increasing concentrations of GuHCl increased the magnitude of the effect of *HUL5* deletion on the stability of RQCsub_{LONG} (from 13.6% to 20.9% to 28.2% at 0, 5, and 10 mM GuHCl respectively; Fig 1G), suggesting that treating *ROLD* cells with GuHCl rescues degradation of RQCsub_{LONG}. Second, the magnitude of bortezomib-induced RQCsub_{LONG} stabilization increased with increasing GuHCl when Hul5 was intact (S2 Fig panel C). This result indicates that the degradation that GuHCl rescued involved both Hul5 and the proteasome. Taken together, these data imply that the aggregation-conducive *ROLD* background impairs CAT tail-mediated degradation, and solubilization of CAT tails rescues this impairment. We thereby posit that CAT tail aggregation antagonizes CAT tail-mediated degradation.

CAT tails exert proteotoxic stress in their aggregated state

To determine how aggregation affects the proteotoxicity of CAT tails, we measured proteotoxic stress after varying CAT tail aggregation propensity (Fig 2A). Proteotoxic stress activates the transcription factor Heat Shock Factor 1 (Hsf1), which then orchestrates transcription of chaperones and other proteostasis-restoring factors [52,53]. Hsf1 activation scales with the magnitude of proteotoxic stress and a previously-published reporter can measure the degree of activation [19]. This reporter consists of GFP under the control of an artificial promoter containing four heat shock elements [54], the consensus binding site for Hsf1 (Fig 2B). *LTN1* deletion alone activated the Hsf1 reporter 2.07-fold relative to wt, while additional *RQC2* overexpression (*ROLD*) led to 22.6-fold activation (Fig 2B). The potent activation observed in

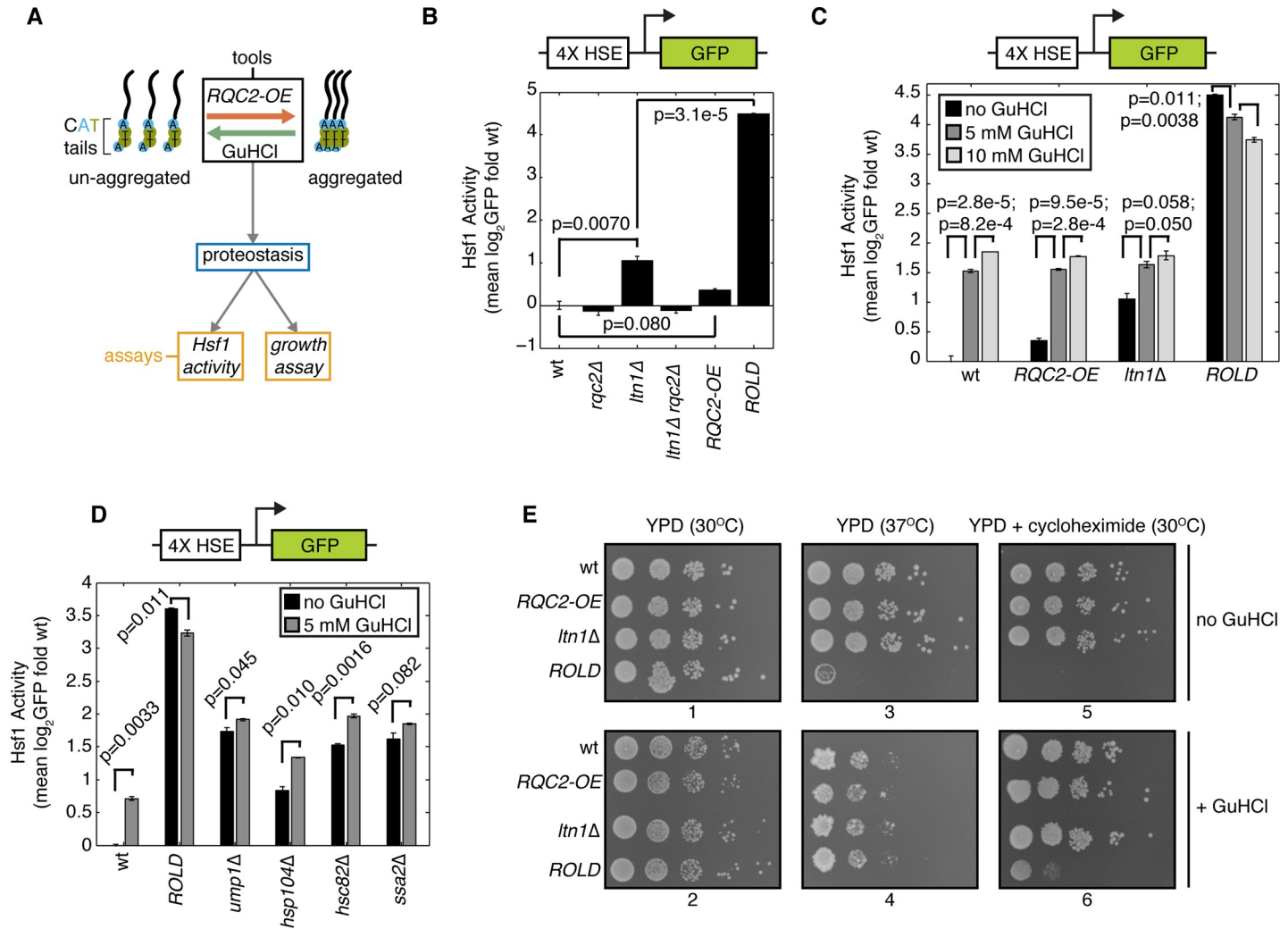


Fig 2. Aggregated CAT tails are proteotoxic. (A) Schematic of experimental approach for assessing how aggregation influences the effect of CAT tails on proteostasis. (B), (C), and (D) Flow cytometry of cells containing an integrated reporter for Hsf1 activation (schematic above). Error bars represent s.e.m. from three independent cultures. P-values from indicated paired t-tests are indicated by lines between bars. HSE, heat shock element. (E) Spot assay of strains grown at 30°C, 37°C, and in 50 ng/ml cycloheximide with and without the presence of 5 mM GuHCl. Plate numbers indicated below images.

<https://doi.org/10.1371/journal.pone.0227841.g002>

the *ROLD* background required *LTN1* deletion, as *RQC2* overexpression in the wt background weakly affected the reporter (Fig 2B). Thus, the combination of *RQC2* overexpression and *LTN1* deletion, which potentiates CAT tail aggregation (S1 Fig panel B) [38], generates a synthetic interaction that results in elevated Hsf1 activity. This increase in Hsf1 activity is consistent with an increase in proteotoxic stress.

If CAT tail aggregation causes proteotoxicity, we reasoned that solubilization of CATylated proteins by GuHCl treatment might reduce this toxicity. GuHCl treatment activated the Hsf1 reporter in a dose-dependent manner in wt, *RQC2-OE*, and *ltn1Δ* strains (Fig 2C), indicating that GuHCl alone exerts some proteotoxic stress in cells. Despite this general activation, GuHCl decreased Hsf1 reporter activation in *ROLD* cells (Fig 2C), suggesting that solubilization of CAT tails alleviates the Hsf1 activation associated with the *ROLD* background. We tested the specificity of this response by measuring the effect of GuHCl on the Hsf1 reporter in other genotypes with high Hsf1 activity [19] (Fig 2D). Hsf1 reporter deactivation was unique

to the *ROLD* condition, as GuHCl increased Hsf1 reporter activation in *ump1Δ*, *hsp104Δ*, and *hsc82Δ* strains and had no significant effect in the *ssa2Δ* strain (Fig 2D). These results suggest that CAT tails exert proteotoxic stress more potently in their aggregated than in their soluble state.

To ensure that our Hsf1 measurements reflect perturbations to proteostasis, we analyzed how CAT tail aggregation affects cells' sensitivity to stressors. At 30°C, all of the strains we examined (wt, *RQC2* overexpression, *ltn1Δ*, and *ROLD*) grew equally well in a spot assay in the absence and presence of 5 mM GuHCl (Fig 2E, plates 1 and 2). This result demonstrates that neither the *ROLD* background nor GuHCl impairs growth in the absence of stress. We then introduced two mild stressors to perturb proteostasis: the thermal stress of 37°C incubation or introduction of 50 ng/ml cycloheximide to increase translational stalling. Neither of these stresses induced a growth defect in the *RQC2-OE* or *ltn1Δ* strains relative to wt (Fig 2E, plates 3 and 5). By contrast, 37°C incubation and 50 ng/ml cycloheximide severely inhibited growth in the *ROLD* strain (Fig 2E, plates 3 and 5). Increased CAT tail aggregation thus co-occurs with sensitivity to thermal and ribosome stalling stresses. Additional GuHCl partially rescued growth of the *ROLD* strain in the presence of cycloheximide (Fig 2E, plate 5 versus plate 6). The combination of GuHCl and 37°C led to a synthetic growth defect in all strains (Fig 2E, plate 3 versus plate 4). Despite this growth defect, the *ROLD* strain grew comparably to wt, *RQC2-OE*, and *ltn1Δ* strains when exposed to both GuHCl and 37°C (Fig 2E, plate 4). Thus, CAT tail aggregation sensitizes cells to mild thermal and ribosome stalling stress. The agreement with our Hsf1 measurements (Fig 2B and 2C) suggests that CAT tail aggregation perturbs proteostasis under the conditions we measured rather than facilitating adaptation to stress.

Disruption of CAT tail aggregation by Pol III perturbation restores CAT tail degradation and alleviates proteotoxicity

Given that GuHCl mildly reduced CAT tail aggregation, we sought an orthogonal perturbation that would more potently inhibit CAT tail aggregation. To find such a perturbation, we screened for mutations that reduced Hsf1 reporter activation in the RQC-compromised *ltn1Δ rps0aΔ* strain, which exhibits Hsf1 hyperactivation [19]. After crossing a genome-wide collection of hypomorphs into this background as well as a wt background via the synthetic genetic array method [41], we found that all reproducible hits other than *RQC2* (whose deletion blocks CATylation) were related to RNA Polymerase III (Pol III). These hits included a non-essential polymerase biogenesis factor, *BUD27* [55], and the essential Pol III subunit *RPC17*. Disruption of each of these by deletion or a “decreased abundance by mRNA perturbation” allele (DAmP) [56] nearly eliminated activation of the Hsf1 reporter in *ROLD* cells compared to wt (S3 Fig panel A). To assess the specificity of this effect to RQC-related Hsf1 activation, we measured the effect of *BUD27* and *RPC17* perturbations in strains with elevated Hsf1 signaling (Fig 3A). Perturbations to *BUD27* and *RPC17* reduced Hsf1 reporter activity in wt, *ump1Δ*, *hsp104Δ*, *hsc82Δ*, and *ssa2Δ* strains (Fig 3A, black versus grey bars). However, the magnitude of this reduction in each strain was substantially less than the 20.7-fold and 13.7-fold reduction we observed in the *ROLD* background after disruption of *BUD27* and *RPC17*, respectively (Fig 3A). Furthermore, Hsf1 reporter activation increased in the Pol III-perturbed backgrounds upon deletion of *UMPI1*, *HSP104*, *HSC82*, and *SSA2* relative to the Pol III-perturbed background strain (S3 Fig panel B). Taken together, these data indicate that Pol III impairment reduces *ROLD*-induced Hsf1 activation without generally preventing Hsf1 activation in other genetic backgrounds.

Because Pol III transcribes target genes like 5S rRNA and tRNAs that play roles in translation [57], we wondered whether Pol III perturbation blocks *ROLD*-induced Hsf1 activation by

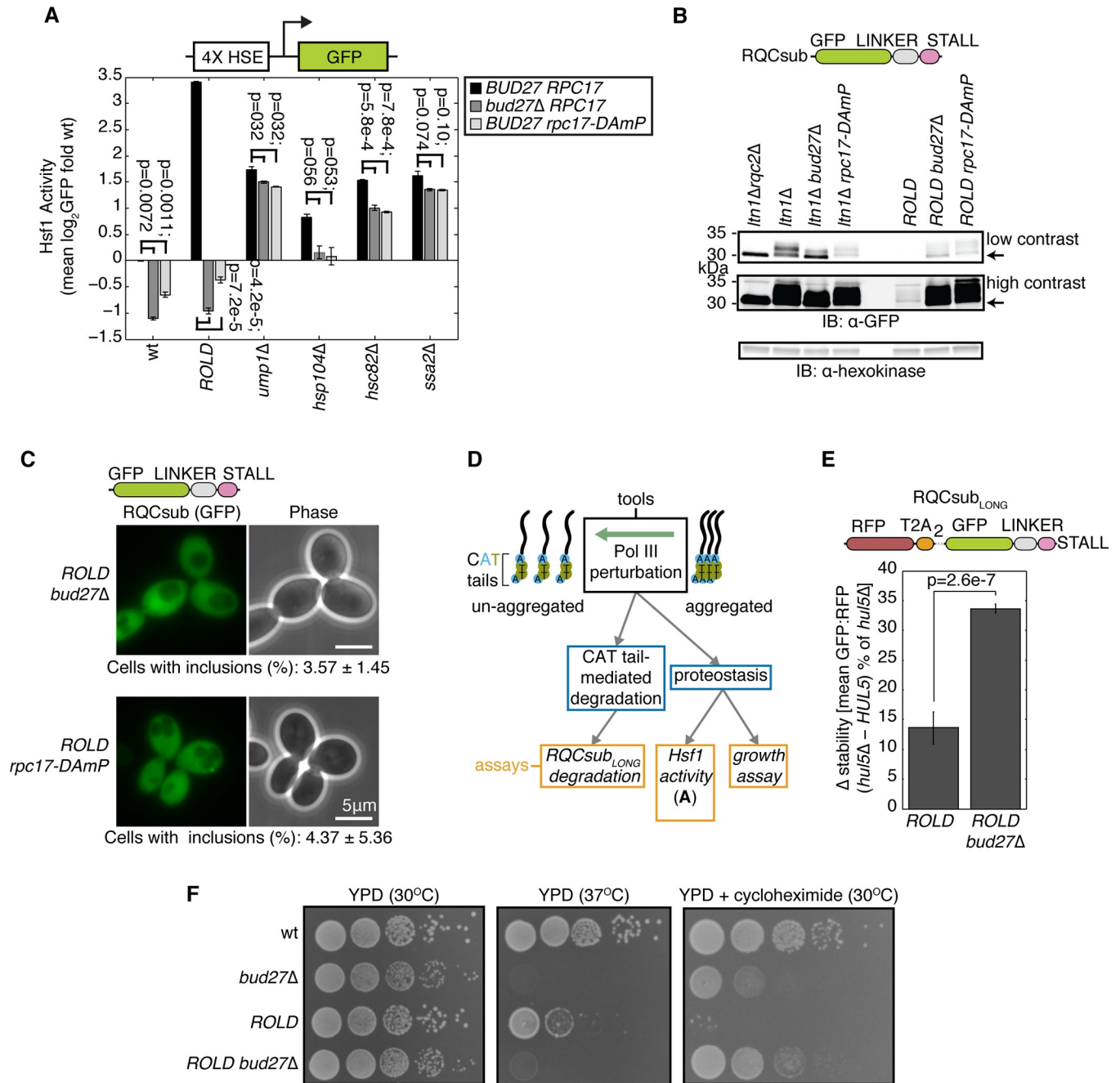


Fig 3. Pol III perturbation inhibits CAT tail aggregation, increases degnon activity, and restores proteostasis. (A) Flow cytometry of cells containing an integrated reporter for Hsf1 activation. Error bars indicate s.e.m. from three independent cultures. P-values from paired t-tests indicated above bars. (B) Whole cell IB of RQCsub expressed in indicated strains. (C) Fluorescence microscopy of cells expressing RQCsub. Percentages of cells containing GFP inclusions reported below micrographs. The micrograph of RQCsub expressed in the *ROLD* strain is shown in Fig 1B. (D) Schematic of experimental strategy for measuring how disruption of aggregation modulates CAT tail-mediated degradation and CAT tails' effect on proteostasis. (E) Δ stability measurements of RQCsub_{LONG} expressed in indicated strains after *HUL5* deletion to quantify CAT tail degnon activity. Error bars as in A. P-value indicates the result of a t-test for particular contrast. (F) Spot assay of cells grown under indicated conditions.

<https://doi.org/10.1371/journal.pone.0227841.g003>

perturbing CAT tail synthesis. Pol III perturbation could block CAT tail synthesis by preventing ribosome stalling, a necessary prerequisite for the RQC pathway to initiate. We evaluated this possibility using a quantitative stalling reporter similar to one previously developed

[11,12] (S3 Fig panel C). *BUD27* deletion did not alleviate stalling induced by (CGN)12 (the stalling sequence in RQCsub) in wt or *ROLD* strains relative to control (S3 Fig panel C). Thus, the effects of Pol III perturbation on translation should not confound our analysis of RQCsub by preventing ribosomes translating RQCsub from stalling. When we monitored RQCsub mobility by SDS-PAGE to directly observe any changes in CAT tails, we observed that RQCsub expressed in the *ltn1Δ bud27Δ* and *ltn1Δ rpc17-DAmP* strains migrated as a smear that was higher in molecular weight compared to the crisp band observed in the CATylation-deficient *ltn1Δ rqc2Δ* strain and lower in molecular weight than the smear observed in the CATylation-competent *ltn1Δ* strain (Fig 3B). In the *ROLD* background, the portion of RQCsub in the resolving gel migrated similarly whether or not we perturbed *BUD27* or *RPC17* (Fig 3B). Additionally, perturbation of *BUD27* and *RPC17* increased the abundance of RQCsub that migrated into the resolving gel (discussed further below) (Fig 3B). Thus, Pol III disruption may decrease the efficiency of CATylation in the *ltn1Δ* background but not in the *ROLD* background.

Given its ability to mitigate Hsf1 hyperactivation in the *ROLD* strain (Fig 3A and S3 Fig panel A) and increase the amount of RQCsub that migrated into a resolving SDS-PAGE gel (Fig 3B), we investigated whether Pol III perturbation could inhibit CAT tail aggregation similarly to GuHCl. *ROLD* cells carrying hypomorphic *BUD27* or *RPC17* alleles formed RQCsub inclusions less frequently (3.57% and 4.37% relative to 56.9% in *ROLD*), consistent with a reduction in CAT tail aggregation (Figs 1B and 3C). Additionally, *BUD27* deletion in the *ROLD* background increased the mobility of RQCsub by SDS-PAGE, reducing the proportion that remained in the well and increasing the proportion that migrated into the resolving gel (S3 Fig panel D). Pol III perturbation thus serves as another tool, in addition to GuHCl, to inhibit CAT tail aggregation.

Given that GuHCl solubilized CAT tails and rescued their degradation in *ROLD* cells (Fig 1C and 1G), we asked whether Pol III perturbation yields the same effect. To quantify CAT tail degradation, we measured RQCsub_{LONG} stability in *ROLD* and *ROLD bud27Δ* cells (Fig 3D). The difference in RQCsub_{LONG} stability (GFP:RFP) in each of these backgrounds with Hul5 (degradation intact) and without Hul5 (degradation blocked) defined the degree of degradation [35]. We validated this approach by demonstrating that the proteasome inhibitor bortezomib did not significantly stabilize RQCsub_{LONG} in *ROLD hul5Δ* and *ROLD bud27Δ hul5Δ* strains (S3 Fig panel E), indicating that *HUL5* deletion blocked degradation in the *ROLD* and *ROLD bud27Δ* backgrounds. *HUL5* deletion stabilized RQCsub_{LONG} in *ROLD bud27Δ* more than in *ROLD* cells (33.7% compared to 13.6%; Fig 3E). In agreement with the effect of GuHCl (Fig 1G), these data demonstrate that limiting CAT tail aggregation by perturbing Pol III restores degradation of CATylated proteins.

We then used Pol III perturbation to analyze how reducing CAT tail aggregation affects proteostasis by determining its effects on growth in the presence of stress (Fig 3D). As previously published, *BUD27* deletion and *rpc17-DAmP* slightly lowered growth rate at 30°C in the wt background (Fig 3F and S3 Fig panel F) [58,59]. *BUD27* deletion strongly impaired growth at 37°C in the wt (previously observed in [58]) and *ROLD* backgrounds (Fig 3F). *rpc17-DAmP* had no effect on the wt strain but restored growth of the *ROLD* strain at 37°C (S3 Fig panel F). Thus, the sensitivity to mild thermal stress caused by *BUD27* deletion renders this perturbation unable to rescue heat sensitivity in the *ROLD* background, but perturbation of Pol III with *rpc17-DAmP* can suppress the *ROLD* strain's sensitivity to heat.

Next, we analyzed the effect of Pol III perturbation on stress induced by the presence of translation inhibitors. Despite causing a growth defect in wt cells, *BUD27* deletion enabled faster growth of *ROLD* cells in the presence of cycloheximide (Fig 3F). Unexpectedly, the growth rate of *ROLD bud27Δ* cells upon cycloheximide exposure was greater than that of the *bud27Δ* strain (Fig 3F). *rpc17-DAmP* had no effect on growth of wt cells in cycloheximide, but

fully rescued growth of *ROLD* cells in cycloheximide (S3 Fig panel F). *BUD27* deletion also rescued growth of the *ROLD* strain in the presence of the translation inhibitor paromomycin, but not hygromycin (S3 Fig panel G). However, *BUD27* deletion alone strongly sensitized growth of wt yeast to hygromycin (S3 Fig panel G) [58], perhaps explaining why this perturbation failed to rescue growth of hygromycin-exposed *ROLD* yeast. Pol III perturbation, similarly to GuHCl, can thereby reduce cells' sensitivity to increased ribosome stalling in addition to inhibiting CAT tail aggregation. Taken together, our observations suggest that improving CAT tail solubility via Pol III perturbation can enhance adaptation to thermal and ribosome stall-inducing stress.

Discussion

We have examined how CAT tail aggregation affects the cell's ability to cope when its burden of incomplete proteins exceeds Ltn1's ability to ubiquitylate them. In cells with compromised Ltn1 function, we modulated the aggregation propensity of CAT tails to determine how aggregation affects the cellular capacity to handle elevated levels of incomplete proteins. Aggregation compromised degradation of CATylated proteins (Fig 1F) and diminished cellular fitness during stress (Fig 2E), while inhibiting aggregation reversed each of these effects (Figs 1G, 2E, 3E and 3F). Our findings suggest that CAT tail aggregation is detrimental, rather than adaptive, in cells with diminished Ltn1 function.

Since their discovery, multiple functions have been attributed to CAT tails. These include a role in assisting Ltn1 activity [27,35,37] and Ltn1-independent roles such as targeting Ltn1-e-vading RQC substrates for degradation [35] or serving as aggregation-inducing post-translational modifications [38]. We previously presented evidence supporting an adaptive, Ltn1-independent function for CAT tails by showing that loss of CAT tails sensitized cells to increased ribosome stalling (cycloheximide) specifically in the absence of Ltn1 [35]. Here we show that this adaptive Ltn1-independent role is unlikely to be CAT tail-mediated aggregation, as aggregation instead increased sensitivity to cycloheximide (Figs 2E and 3F). Combined with the recent finding that CAT tail degron function is shared with prokaryotic Ala tails [24], our results suggest that marking escaped RQC substrates for degradation is the primary function of CAT tails.

Our findings elevate the question of why yeast and metazoan CAT tails have retained their threonine content, and thereby aggregation propensity, through evolution. We propose two models to explain this. In the first model, CAT tail aggregation facilitates adaptation to an as-of-yet untested stress with evolutionary relevance. The tools we used here to control aggregation may prove useful in probing this model by systematically assessing the fitness benefit of CAT tail aggregation in diverse conditions. The second model proposes that the inclusion of threonine in CAT tails facilitates a function of CAT tails other than aggregation. For instance, threonine incorporation could produce more potent CAT tail degrons, assist in Ltn1-mediated ubiquitylation, or aid in mounting a protective heat shock response. To preserve threonine content, the fitness benefit from this threonine-mediated CAT tail function would need to outweigh any fitness deficits arising from CAT tail aggregation. Given the recent discovery of Rqc2 homologs that incorporate different amino acids into CAT tails [24,34], domain-swapping between these homologs to bias CAT tail amino acid content may assist in determining the function of threonine in CAT tails in future studies. Broadly, understanding how the variable amino acid composition of CAT tails has evolved to meet physiological demands in different organisms may prove a fruitful area of research.

We exploited *RQC2* overexpression and Pol III disruption as tools to genetically modify CAT tail aggregation. While these proved useful in analyzing CAT tails in their aggregated and

un-aggregated states, the underlying mechanism behind these perturbations is not the focus of this study (nor does it influence our conclusions) and remains unclear. *RQC2* overexpression has been proposed to enhance aggregation because endogenous Rqc2 is limiting for CATylation [38]. Under such a scenario, *RQC2* overexpression would enable CATylation of more escaped RQC substrates that could then nucleate CAT tail aggregates. Although pleiotropic [57], Pol III perturbation could function in the opposite manner. By limiting translation initiation [58], Pol III perturbation could decrease the total amount of CATylated proteins in the cell and thereby disfavor nucleation of CAT tail aggregation. Alternatively, Pol III perturbation may alter the cellular pool of tRNAs and, thereby, the tRNAs that Rqc2 recruits to synthesize CAT tails. Indeed, disruption of Pol III altered the mobility of soluble CAT tails by SDS-PAGE (Fig 3B, lanes 3 and 4 compared to lane 2), indicative of a change in composition. The altered composition of CAT tails under Pol III-perturbed conditions may improve their solubility. Further studies will be needed to decipher the mechanisms by which these perturbations alleviate CAT tail aggregation.

We report here that CAT tail aggregation modifies the toxicity associated with disrupted Ltn1 function. In mice, a hypomorphic *LTN1* allele induces a progressive neurodegeneration that shares phenotypic similarities with amyotrophic lateral sclerosis (ALS) [32]. It is possible that degenerating neurons in these *LTN1*-hypomorphic mice harbor toxic CAT tail aggregates, as has been observed in a *Drosophila* model of Parkinson Disease [34]. As the connection between the phenotypes in these disease models and human disease becomes more clear, future studies can focus on strategies to mitigate toxicity associated with compromised Ltn1. Our study serves as a proof-of-principle that disrupting CAT tail aggregation lessens this toxicity.

Supporting information

S1 Fig. *RQC2* overexpression and guanidinium hydrochloride are tools to control CAT tail aggregation. (A) Flow cytometry of cells expressing Rqc2-RFP to assess the degree of Rqc2 overproduction by the *TDH3* promoter. Error bars represent s.e.m. from three independent cultures. (B) Lysate IB of RQCsub expressed in *ltn1Δ* compared to *ROLD*. (C) Immunoblot of RQCsub immunoprecipitated from *ltn1Δ* and *ROLD* lysates with and without tobacco etch virus (TEV) protease treatment. Arrow denotes molecular weight of non-CATylated RQCsub. Asterisk indicates the full-length RQCsub protein product, produced when ribosomes translate through the stall sequence (region past the stall not pictured in schematic). (D) Microscopy of RQCsub expressed in *ROLD* grown in various concentrations of guanidinium hydrochloride (GuHCl). (TIF)

S2 Fig. Supporting data for the effect of aggregation of CAT tail-mediated degradation. (A) Flow cytometry of cells expressing RQCsub_{LONG}. Error bars indicate s.e.m. from three independent cultures. (B) and (C) Additional data to support Fig 1F–1G. Stability measurements of RQCsub_{LONG} expressed in *ROLD* cells grown in indicated GuHCl concentrations with additional bortezomib treatment to inhibit the proteasome and *HUL5* deletion to measure CAT tail degron activity. Error bars as in A. P-values are indicated above bars. Thick lines indicate paired t-tests, probing the significance of bortezomib (btz)-induced stabilization. Thin lines denote t-tests for particular contrast, measuring how significantly different *HUL5* deletion-induced stabilization is under different conditions. (TIF)

S3 Fig. Effects of Pol III perturbation on Hsf1 activation, stalling, and CAT tail degron activity. (A) Flow cytometry of cells containing an integrated reporter for Hsf1 activation.

Error bars indicate s.e.m. from three independent cultures. P-values from paired t-tests indicated above bars. (B) Flow cytometry of Pol III-perturbed cells containing an integrated reporter for Hsf1 activation. These data are also contained in Fig 3A, but are reordered here to simplify comparisons within two Pol III-perturbed genetic backgrounds. Error bars as in A. (C) Above, schematic of stalling reporter with the same (CGN)12 stalling sequence contained in RQCsub or a non-stalling (Ser-Thr)6 sequence, similar to a reporter used in refs 11 and 12. Below, flow cytometry of stalling and non-stalling reporters expressed in indicated strains. Error bars as in A. (D) IB of lysates containing RQCsub derived from *ROLD* compared to *ROLD bud27Δ*. (E) Additional data to support Fig 3E. Stability measurements of RQCsub_{LONG} expressed in indicated strains with bortezomib (btz) treatment to inhibit the proteasome and *HUL5* deletion to block CAT tail degon activity. Error bars indicate s.e.m. from three independent cultures. P-values are given above bars. Results of paired t-tests measuring the significance of bortezomib-induced stabilization are indicated with thick lines. The result of a t-test for particular contrast is indicated with thin lines; this assesses how significantly different *HUL5* deletion-induced stabilization is in *ROLD* compared to *ROLD bud27Δ*. (F and G) Spot assay of yeast strains grown under indicated conditions.

(TIF)

S1 Table. Yeast strains used in this study.

(PDF)

S2 Table. Plasmids used in this study.

(PDF)

S1 Dataset. Results from Hsf1 screen. Each row includes the name of a gene (column 1) that was disrupted with a hypomorphic allele (deletion for non-essential genes and DAmP for essential genes) and measured in a strain with a GFP-fluorescent Hsf1 reporter in either a wt (column 2) or *ltn1Δ rps0aΔ* background (column 3). The interaction (difference) between these measurements is reported in column 4.

(XLS)

S1 Raw Images. Uncropped images of immunoblots contained in the main and supplementary figures.

(TIF)

Acknowledgments

We thank D. Pincus, D. Jarosz, R. Kopito, B. Lu, Z. Wu, E.P. Geiduschek, and the members of the Brandman lab for helpful suggestions. We thank the Theriot and Straight labs (Stanford University) for the use of their microscopes. We thank J. Weissman and D. Wong for facilitating the screen for suppressors of RQC-mediated Hsf1 activation.

Author Contributions

Conceptualization: Cole S. Sitron, Joseph H. Park, Onn Brandman.

Data curation: Cole S. Sitron, Joseph H. Park, Onn Brandman.

Formal analysis: Cole S. Sitron, Joseph H. Park, Onn Brandman.

Funding acquisition: Onn Brandman.

Investigation: Cole S. Sitron, Joseph H. Park, Jenna M. Giafaglione, Onn Brandman.

Methodology: Cole S. Sitron, Joseph H. Park, Jenna M. Giafaglione, Onn Brandman.

Project administration: Onn Brandman.

Resources: Onn Brandman.

Software: Cole S. Sitron, Joseph H. Park, Onn Brandman.

Supervision: Onn Brandman.

Validation: Cole S. Sitron, Joseph H. Park, Jenna M. Giafaglione, Onn Brandman.

Visualization: Cole S. Sitron, Joseph H. Park, Jenna M. Giafaglione, Onn Brandman.

Writing – original draft: Cole S. Sitron, Joseph H. Park, Onn Brandman.

Writing – review & editing: Cole S. Sitron, Joseph H. Park, Jenna M. Giafaglione, Onn Brandman.

References

1. Moore SD, Sauer RT. The tmRNA system for translational surveillance and ribosome rescue. *Annu Rev Biochem.* 2007; 76: 101–124. <https://doi.org/10.1146/annurev.biochem.75.103004.142733> PMID: 17291191
2. Brandman O, Hegde RS. Ribosome-associated protein quality control. *Nat Struct Mol Biol.* 2016; 23: 7–15. <https://doi.org/10.1038/nsmb.3147> PMID: 26733220
3. Defenouillère Q, Fromont-Racine M. The ribosome-bound quality control complex: from aberrant peptide clearance to proteostasis maintenance. *Current Genetics.* 2017. pp. 997–1005. <https://doi.org/10.1007/s00294-017-0708-5> PMID: 28528489
4. Ikeuchi K, Izawa T, Inada T. Recent Progress on the Molecular Mechanism of Quality Controls Induced by Ribosome Stalling. *Front Genet.* 2018; 9: 743. <https://doi.org/10.3389/fgene.2018.00743> PMID: 30705686
5. Joazeiro CAP. Mechanisms and functions of ribosome-associated protein quality control. *Nat Rev Mol Cell Biol.* 2019; 20: 368–383. <https://doi.org/10.1038/s41580-019-0118-2> PMID: 30940912
6. Simms CL, Yan LL, Zaher HS. Ribosome Collision Is Critical for Quality Control during No-Go Decay. *Mol Cell.* 2017; 68: 361–373.e5. <https://doi.org/10.1016/j.molcel.2017.08.019> PMID: 28943311
7. Juszkiwicz S, Chandrasekaran V, Lin Z, Kraatz S, Ramakrishnan V, Hegde RS. ZNF598 Is a Quality Control Sensor of Collided Ribosomes. *Mol Cell.* 2018; 72: 469–481.e7. <https://doi.org/10.1016/j.molcel.2018.08.037> PMID: 30293783
8. Ikeuchi K, Tesina P, Matsuo Y, Sugiyama T, Cheng J, Saeki Y, et al. Collided ribosomes form a unique structural interface to induce Hel2-driven quality control pathways. *EMBO J.* 2019; 38: e100276. <https://doi.org/10.15252/embj.2018100276> PMID: 30609991
9. Tsuboi T, Kuroha K, Kudo K, Makino S, Inoue E, Kashima I, et al. Dom34:hbs1 plays a general role in quality-control systems by dissociation of a stalled ribosome at the 3' end of aberrant mRNA. *Mol Cell.* 2012; 46: 518–529. <https://doi.org/10.1016/j.molcel.2012.03.013> PMID: 22503425
10. Shao S, von der Malsburg K, Hegde RS. Listerin-dependent nascent protein ubiquitination relies on ribosome subunit dissociation. *Mol Cell.* 2013; 50: 637–648. <https://doi.org/10.1016/j.molcel.2013.04.015> PMID: 23685075
11. Sundaramoorthy E, Leonard M, Mak R, Liao J, Fulzele A, Bennett EJ. ZNF598 and RACK1 Regulate Mammalian Ribosome-Associated Quality Control Function by Mediating Regulatory 40S Ribosomal Ubiquitylation. *Mol Cell.* 2017; 65: 751–760.e4. <https://doi.org/10.1016/j.molcel.2016.12.026> PMID: 28132843
12. Juszkiwicz S, Hegde RS. Initiation of Quality Control during Poly(A) Translation Requires Site-Specific Ribosome Ubiquitination. *Mol Cell.* 2017; 65: 743–750.e4. <https://doi.org/10.1016/j.molcel.2016.11.039> PMID: 28065601
13. Matsuo Y, Ikeuchi K, Saeki Y, Iwasaki S, Schmidt C, Udagawa T, et al. Ubiquitination of stalled ribosome triggers ribosome-associated quality control. *Nat Commun.* 2017; 8: 159. <https://doi.org/10.1038/s41467-017-00188-1> PMID: 28757607
14. Shoemaker CJ, Eyler DE, Green R. Dom34:Hbs1 promotes subunit dissociation and peptidyl-tRNA drop-off to initiate no-go decay. *Science.* 2010; 330: 369–372. <https://doi.org/10.1126/science.1192430> PMID: 20947765

15. Pisareva VP, Skabkin MA, Hellen CUT, Pestova TV, Pisarev AV. Dissociation by Pelota, Hbs1 and ABCE1 of mammalian vacant 80S ribosomes and stalled elongation complexes. *EMBO J*. 2011; 30: 1804–1817. <https://doi.org/10.1038/emboj.2011.93> PMID: 21448132
16. Lyumkis D, dos Passos DO, Tahara EB, Webb K, Bennett EJ, Vinterbo S, et al. Structural basis for translational surveillance by the large ribosomal subunit-associated protein quality control complex. *Proceedings of the National Academy of Sciences*. 2014; 111: 15981–15986.
17. Sitron CS, Park JH, Brandman O. Asc1, Hel2, and Slh1 couple translation arrest to nascent chain degradation. *RNA*. 2017; 23: 798–810. <https://doi.org/10.1261/ma.060897.117> PMID: 28223409
18. Bengtson MH, Joazeiro CAP. Role of a ribosome-associated E3 ubiquitin ligase in protein quality control. *Nature*. 2010; 467: 470–473. <https://doi.org/10.1038/nature09371> PMID: 20835226
19. Brandman O, Stewart-Ornstein J, Wong D, Larson A, Williams CC, Li G-W, et al. A ribosome-bound quality control complex triggers degradation of nascent peptides and signals translation stress. *Cell*. 2012; 151: 1042–1054. <https://doi.org/10.1016/j.cell.2012.10.044> PMID: 23178123
20. Defenouillère Q, Yao Y, Mouaikel J, Namane A, Galopier A, Decourty L, et al. Cdc48-associated complex bound to 60S particles is required for the clearance of aberrant translation products. *Proc Natl Acad Sci U S A*. 2013; 110: 5046–5051. <https://doi.org/10.1073/pnas.1221724110> PMID: 23479637
21. Verma R, Oania RS, Kolawa NJ, Deshaies RJ. Cdc48/p97 promotes degradation of aberrant nascent polypeptides bound to the ribosome. *Elife*. 2013; 2: e00308. <https://doi.org/10.7554/eLife.00308> PMID: 23358411
22. Abo T, Ueda K, Sunohara T, Ogawa K, Aiba H. SsrA-mediated protein tagging in the presence of mis-coding drugs and its physiological role in *Escherichia coli*. *Genes to Cells*. 2002. pp. 629–638. <https://doi.org/10.1046/j.1365-2443.2002.00549.x> PMID: 12081641
23. Moore SD, Sauer RT. Ribosome rescue: tmRNA tagging activity and capacity in *Escherichia coli*. *Mol Microbiol*. 2005; 58: 456–466. <https://doi.org/10.1111/j.1365-2958.2005.04832.x> PMID: 16194232
24. Lytvynenko I, Paternoga H, Thrun A, Balke A, Müller TA, Chiang CH, et al. Alanine Tails Signal Proteolysis in Bacterial Ribosome-Associated Quality Control. *Cell*. 2019; 178: 76–90.e22. <https://doi.org/10.1016/j.cell.2019.05.002> PMID: 31155236
25. Oussenko IA, Abe T, Ujiie H, Muto A, Bechhofer DH. Participation of 3'-to-5' exoribonucleases in the turnover of *Bacillus subtilis* mRNA. *J Bacteriol*. 2005; 187: 2758–2767. <https://doi.org/10.1128/JB.187.8.2758-2767.2005> PMID: 15805522
26. Choe Y-J, Park S-H, Hassemer T, Körner R, Vincenz-Donnelly L, Hayer-Hartl M, et al. Failure of RQC machinery causes protein aggregation and proteotoxic stress. *Nature*. 2016; 531: 191–195. <https://doi.org/10.1038/nature16973> PMID: 26934223
27. Kostova KK, Hickey KL, Osuna BA, Hussmann JA, Frost A, Weinberg DE, et al. CAT-tailing as a fail-safe mechanism for efficient degradation of stalled nascent polypeptides. *Science*. 2017; 357: 414–417. <https://doi.org/10.1126/science.aam7787> PMID: 28751611
28. Glass JI, Assad-Garcia N, Alperovich N, Yoeseff S, Lewis MR, Maruf M, et al. Essential genes of a minimal bacterium. *Proc Natl Acad Sci U S A*. 2006; 103: 425–430. <https://doi.org/10.1073/pnas.0510013103> PMID: 16407165
29. Chaudhuri RR, Allen AG, Owen PJ, Shalom G, Stone K, Harrison M, et al. Comprehensive identification of essential *Staphylococcus aureus* genes using Transposon-Mediated Differential Hybridisation (TMDH). *BMC Genomics*. 2009; 10: 291. <https://doi.org/10.1186/1471-2164-10-291> PMID: 19570206
30. Julio SM, Heithoff DM, Mahan MJ. *ssrA* (tmRNA) Plays a Role in *Salmonella enterica* Serovar Typhimurium Pathogenesis. *J Bacteriol*. 2000; 182: 1558–1563. <https://doi.org/10.1128/jb.182.6.1558-1563.2000> PMID: 10692360
31. Mann B, van Opijnen T, Wang J, Obert C, Wang Y-D, Carter R, et al. Control of virulence by small RNAs in *Streptococcus pneumoniae*. *PLoS Pathog*. 2012; 8: e1002788. <https://doi.org/10.1371/journal.ppat.1002788> PMID: 22807675
32. Chu J, Hong NA, Masuda CA, Jenkins BV, Nelms KA, Goodnow CC, et al. A mouse forward genetics screen identifies LISTERIN as an E3 ubiquitin ligase involved in neurodegeneration. *Proc Natl Acad Sci U S A*. 2009; 106: 2097–2103. <https://doi.org/10.1073/pnas.0812819106> PMID: 19196968
33. Ishimura R, Nagy G, Dotu I, Zhou H, -L. Yang X, Schimmel P, et al. Ribosome stalling induced by mutation of a CNS-specific tRNA causes neurodegeneration. *Science*. 2014; 345: 455–459. <https://doi.org/10.1126/science.1249749> PMID: 25061210
34. Wu Z, Tantray I, Lim J, Chen S, Li Y, Davis Z, Sitron C, Dong J, Gispert S, Auburger G, Brandman O, Bi X, Snyder M, Lu B. MISTERMINATE Mechanistically Links Mitochondrial Dysfunction with Proteostasis Failure. *Mol Cell*. 2019; 75: 835–848. <https://doi.org/10.1016/j.molcel.2019.06.031> PMID: 31378462
35. Sitron CS, Brandman O. CAT tails drive degradation of stalled polypeptides on and off the ribosome. *Nat Struct Mol Biol*. 2019; 26: 450–459. <https://doi.org/10.1038/s41594-019-0230-1> PMID: 31133701

36. Shen PS, Park J, Qin Y, Li X, Parsawar K, Larson MH, et al. Protein synthesis. Rqc2p and 60S ribosomal subunits mediate mRNA-independent elongation of nascent chains. *Science*. 2015; 347: 75–78. <https://doi.org/10.1126/science.1259724> PMID: 25554787
37. Osuna BA, Howard CJ, Kc S, Frost A, Weinberg DE. In vitro analysis of RQC activities provides insights into the mechanism and function of CAT tailing. *Elife*. 2017; e27949. <https://doi.org/10.7554/eLife.27949> PMID: 28718767
38. Yonashiro R, Tahara EB, Bengtson MH, Khokhrina M, Lorenz H, Chen K-C, et al. The Rqc2/Tae2 subunit of the ribosome-associated quality control (RQC) complex marks ribosome-stalled nascent polypeptide chains for aggregation. *Elife*. 2016; 5: e11794. <https://doi.org/10.7554/eLife.11794> PMID: 26943317
39. Defenouillère Q, Zhang E, Namane A, Mouaikel J, Jacquier A, Fromont-Racine M. Rqc1 and Ltn1 prevent CAT-tail induced protein aggregation by efficient recruitment of Cdc48 on stalled 60S subunits. *J Biol Chem*. 2016; 291: 12245–12253. <https://doi.org/10.1074/jbc.M116.722264> PMID: 27129255
40. Edelstein A, Amodaj N, Hoover K, Vale R, Stuurman N. Computer Control of Microscopes Using μ Manager. *Current Protocols in Molecular Biology*. 2010. <https://doi.org/10.1002/0471142727.mb1420s92> PMID: 20890901
41. Tong AH, Evangelista M, Parsons AB, Xu H, Bader GD, Pagé N, et al. Systematic genetic analysis with ordered arrays of yeast deletion mutants. *Science*. 2001; 294: 2364–2368. <https://doi.org/10.1126/science.1065810> PMID: 11743205
42. Letzring DP, Dean KM, Grayhack EJ. Control of translation efficiency in yeast by codon–anticodon interactions. *RNA*. 2010; 16: 2516–2528. <https://doi.org/10.1261/ma.2411710> PMID: 20971810
43. Eaglestone SS, Ruddock LW, Cox BS, Tuite MF. Guanidine hydrochloride blocks a critical step in the propagation of the prion-like determinant [PSI⁺] of *Saccharomyces cerevisiae*. *Proc Natl Acad Sci U S A*. 2000; 97: 240–244. <https://doi.org/10.1073/pnas.97.1.240> PMID: 10618402
44. Ness F, Ferreira P, Cox BS, Tuite MF. Guanidine Hydrochloride Inhibits the Generation of Prion “Seeds” but Not Prion Protein Aggregation in Yeast. *Mol Cell Biol*. 2002; 22: 5593–5605. <https://doi.org/10.1128/MCB.22.15.5593-5605.2002> PMID: 12101251
45. Byrne LJ, Cox BS, Cole DJ, Ridout MS, Morgan BJT, Tuite MF. Cell division is essential for elimination of the yeast [PSI⁺] prion by guanidine hydrochloride. *Proc Natl Acad Sci U S A*. 2007; 104: 11688–11693. <https://doi.org/10.1073/pnas.0701392104> PMID: 17606924
46. Ferreira PC, Ness F, Edwards SR, Cox BS, Tuite MF. The elimination of the yeast [PSI⁺] prion by guanidine hydrochloride is the result of Hsp104 inactivation. *Mol Microbiol*. 2001; 40: 1357–1369. <https://doi.org/10.1046/j.1365-2958.2001.02478.x> PMID: 11442834
47. Jung G, Masison DC. Guanidine hydrochloride inhibits Hsp104 activity in vivo: a possible explanation for its effect in curing yeast prions. *Curr Microbiol*. 2001; 43: 7–10. <https://doi.org/10.1007/s002840010251> PMID: 11375656
48. Jung G, Jones G, Masison DC. Amino acid residue 184 of yeast Hsp104 chaperone is critical for prion-curing by guanidine, prion propagation, and thermotolerance. *Proc Natl Acad Sci U S A*. 2002; 99: 9936–9941. <https://doi.org/10.1073/pnas.152333299> PMID: 12105276
49. Grimminger V, Richter K, Imhof A, Buchner J, Walter S. The prion curing agent guanidinium chloride specifically inhibits ATP hydrolysis by Hsp104. *J Biol Chem*. 2004; 279: 7378–7383. <https://doi.org/10.1074/jbc.M312403200> PMID: 14668331
50. Donnelly MLL, Ryan MD, Mehrotra A, Gani D, Hughes LE, Luke G, et al. Analysis of the aphthovirus 2A/2B polyprotein “cleavage” mechanism indicates not a proteolytic reaction, but a novel translational effect: a putative ribosomal “skip.” *Journal of General Virology*. 2001. pp. 1013–1025. <https://doi.org/10.1099/0022-1317-82-5-1013> PMID: 11297676
51. Szymczak AL, Vignali DAA. Development of 2A peptide-based strategies in the design of multicistronic vectors. *Expert Opin Biol Ther*. 2005; 5: 627–638. <https://doi.org/10.1517/14712598.5.5.627> PMID: 15934839
52. Åkerfelt M, Trouillet D, Mezger V, Sistonen LEA. Heat shock factors at a crossroad between stress and development. *Ann N Y Acad Sci*. 2007; 1113: 15–27. <https://doi.org/10.1196/annals.1391.005> PMID: 17483205
53. Morimoto RI. The heat shock response: systems biology of proteotoxic stress in aging and disease. *Cold Spring Harb Symp Quant Biol*. 2011; 76: 91–99. <https://doi.org/10.1101/sqb.2012.76.010637> PMID: 22371371
54. Sorger PK, Pelham HR. Purification and characterization of a heat-shock element binding protein from yeast. *EMBO J*. 1987; 6: 3035–3041. PMID: 3319580
55. Mirón-García MC, Garrido-Godino AI, García-Molinero V, Hernández-Torres F, Rodríguez-Navarro S, Navarro F. The prefoldin bud27 mediates the assembly of the eukaryotic RNA polymerases in an rpb5-

- dependent manner. *PLoS Genet.* 2013; 9: e1003297. <https://doi.org/10.1371/journal.pgen.1003297> PMID: [23459708](https://pubmed.ncbi.nlm.nih.gov/23459708/)
56. Yan Z, Costanzo M, Heisler LE, Paw J, Kaper F, Andrews BJ, et al. Yeast Barcoders: a chemogenomic application of a universal donor-strain collection carrying bar-code identifiers. *Nature Methods.* 2008. pp. 719–725. <https://doi.org/10.1038/nmeth.1231> PMID: [18622398](https://pubmed.ncbi.nlm.nih.gov/18622398/)
 57. Turowski TW, Tollervey D. Transcription by RNA polymerase III: insights into mechanism and regulation. *Biochem Soc Trans.* 2016; 44: 1367–1375. <https://doi.org/10.1042/BST20160062> PMID: [27911719](https://pubmed.ncbi.nlm.nih.gov/27911719/)
 58. Deplazes A, Möckli N, Luke B, Auerbach D, Peter M. Yeast Uri1p promotes translation initiation and may provide a link to cotranslational quality control. *EMBO J.* 2009; 28: 1429–1441. <https://doi.org/10.1038/emboj.2009.98> PMID: [19387492](https://pubmed.ncbi.nlm.nih.gov/19387492/)
 59. Breslow DK, Cameron DM, Collins SR, Schuldiner M, Stewart-Ornstein J, Newman HW, et al. A comprehensive strategy enabling high-resolution functional analysis of the yeast genome. *Nat Methods.* 2008; 5: 711–718. <https://doi.org/10.1038/nmeth.1234> PMID: [18622397](https://pubmed.ncbi.nlm.nih.gov/18622397/)